Journal of Porous Materials (2023) 30:55–64
https://doi.org/10.1007/s10934-022-01325-y

Oxidation of furfural to bio-based molecules with hydrogen peroxide via modified layered double hydroxides: the effect of gold nanoparticles on the selectivity

Ghezlane Berrahou-Harchaoui[1] · Redouane Bachir[1] · Sumeya Bedrane[1] · Jose Juan Calvino[2] · Juan Carlos Hernandez Garrido[2]

Accepted: 5 August 2022 / Published online: 10 August 2022

Abstract
The aim of this article is to study the catalytic capacities of gold nanoparticles based on a layered double hydroxide prepared by a depo-precipitation method in oxidation. The main interest of this work is to prove the possibility of using these materials as catalysis for selective oxidation for succinic acid production. The textural and morphological properties were obtained by several analysis techniques such as: X-ray diffraction, Infrared spectroscopy, Nitrogen adsorption–desorption, Scanning electron microscopy, Diffuse-Reflectance UV–Visible and High-resolution transmission electron microscopy. The characterization results obtained showed a very well-structured layered double hydroxide with small gold nanoparticles supported on surface. However, the catalytic performance of these new materials was studied in the furfural oxidation with hydrogen peroxide. The use of gold nanoparticles supported layered double hydroxide exhibited a beneficial effect on selectivity giving an exclusive selectivity in succinic acid.

Keywords Hydroxide double lamellar · Gold nanoparticles · Furfural oxidation · Succinic acid · Hydrogen peroxide

1 Introduction

The transformation of lignocellulosic biomass into a platform molecule, (e.g. 5-hydroxymethylfurfural, furfural, levulinic acid, fumaric acid and succinic acid [1–3]), allows the synthesis of a large number of high value added products used to replace fuels [4, 5]. Among these molecules, as stated by the United States Department of Energy [6], succinic acid is the one of the most important platform biomolecule having a very broad industrial application in food, cosmetic, pharmaceutical and plastic production [7, 8].Succinic acid is also used as a raw material for the synthesis of various basic chemicals, biopolymers [3, 9, 10], solvents [11] and biodegradable polymers, such as polybutylene succinate adipate and polybutylene succinate [12]. Currently, much of the commercial succinic acid has been produced by conventional petrochemical processes, by a catalytic hydrogenation of maleic anhydride previously produced by the catalytic oxidation of hydrocarbons (benzene and butane) and by a microbial fermentation processes of many biomass substrates exploited for its the production. Nevertheless, these processes require meticulous fermentation conditions as well as complex steps to separate succinic acid from the fermentation broth [13, 14].

Since the last decade, several researchers have attempted to find an alternative to the production of succinic acid from biomass-derived compounds, such as furfural and furan derivatives [1, 13, 15] by oxidation using different oxidizing agents under moderate conditions.

Focusing on this research angle, Choudhary et al., studied the use of hydrogen peroxide as an oxidizing agent in the production of succinic acid from furfural oxidation with homogeneous and heterogeneous catalysis [1, 16]. They found that the use of P-toluene-sulfonic acid as homogeneous catalysis has a great catalytic activity, and the use

✉ Ghezlane Berrahou-Harchaoui
ghezlane.berrahou@univ-tlemcen.dz;
ghezlaneberrahou@yahoo.fr

[1] Laboratory of Catalysis and Synthesis in Organic Chemistry (LCSCO), University of Tlemcen Algeria, Imama BP119, 13000 Tlemcen, Algeria

[2] Departamento de Ciencia de los Materiales, Ingeniería Metalúrgica Y Química Inorgánica, Facultad de Ciencias, Universidad de Cádiz, Campus Río San Pedro, 11510 Puerto Real Cádiz, Spain

of heterogeneous catalysis like commercial Amberlyst-15 gives succinic acid yields of 74% at 80 °C for a 24-h reaction time. Also, Kingkaew et al., investigated furfural oxidation with peroxide hydrogen and Dowex-G26 as catalyst [17] and concluded that 75% of succinic acid was obtained at 80 °C under a moderate reaction condition.

The choice of hydrogen peroxide makes it the best oxidizing agent taking into account the fact that it is cheap, ecological, environmentally friendly and with high oxygen content [1, 18–20]. The challenge is**;** therefore**,** to find a catalyst that can be easily prepared, stable, with low-cost, and used to improve succinic acid production in the oxidation reaction.

This present research aims to investigate the production of succinic acid by furfural oxidation with hydrogen peroxide by means of new gold nanoparticles supported layered double hydroxides as catalyst.

The Layered double hydroxides (LDH) are known as anionic clays. They consist of a positively charged edge sharing octahedral and form brucite-like host layers. The net positive charges on the layers are balanced by exchangeable anions intercalated between the sheets [21]. Their structure is described by stacking sheets of $M(OH)_2$ composition which consists of octahedral M^{2+} cation surrounded by OH^- hydroxyl groups. These octahedral units are stuck by the edges forming infinite layers, with OH^- bonds perpendicular to the plane of the layers [22, 23]. In the LDH phases, M^{3+} cations substitute a portion of the M^{2+} cations in the layers, thereby inducing the positively charged leaflets. The positive charge excess is compensated by anions and water molecules present in the interfering space allowing electro-neutrality [24]. The LDH adopt the following formula: $[M^{2+}_{1-x}\, M^{3+}_{x}(OH)_2]^{x+}\, [An^{n-}]_{x/n}$, m H_2O. Where M^{2+} and M^{3+} are the divalent (Ni^{2+}, Mg^{2+}, Cu^{2+}, Zn^{2+}, Co^{2+} etc..) and trivalent (Al^{3+}, Cr^{3+}, Fe^{3+}, Ti^{3+} etc.) metal cations, respectively, and A^{n-} is the exchangeable interlayer (CO_3^{2-}, NO_3^-, Cl^-, SO_4^{2-}, etc.…) anion [21, 25]. LDH have received a lot of attention in recent years because of their potential utility as adsorbents and anion exchangers [21], in electrochemical reactions, medicine [26], photocatalysis [27], as basic catalysts [28, 29] and more importantly as catalyst supports [30].These applications are dependent on their layered structure, surface area, porosity and granular distribution [31].

The possibility of using LDH as supports for gold nanoparticles at low temperature reactions has attracted a big interest since the pioneering work of Haruta et al. which revealed a high activity of oxidation using gold supported nanoparticles on various metal oxides [32].

Gold nanoparticles supported on solids with high surface area are used for a large variety of catalytic reactions with industrial and environmental importance**,** such as cyclohexene oxidation [33–35], CO oxidation [23],benzyl alcohol oxidation [36], adsorption [37], photocatalysis [38],organic synthesis [39, 40], organic contaminants oxidation [41] and furfural oxidation [42]. The solids support materials play the role of stabilizing gold nanoparticles at different oxidation states and controlling their dispersion level as nanoparticles size [43].

Among the numerous materials, layered double hydroxides (LDH) exhibit unique features which are not found in other solid supports if used as support materials for gold nanoparticles, thereby making Au/LDH composites a specific catalyst [42]. Taking advantages of their unique tunable properties, LDH are suitable to manufacture Au/LDH composites.

In this work, we investigated facile routes at room temperature to obtain novel Ni_xAl-LDH as the support of Au/Ni_xAl-LDH catalyst for furfural oxidation. Initially, we synthesized Ni_xAl-LDH with various metals loading by coprecipitation at pH constant method. Gold nanoparticles were then immobilized on the support by using the deposition precipitation method. X-ray diffraction, Infrared spectroscopy, Nitrogen adsorption–desorption, Scanning electron microscopy, Diffuse-Reflectance UV–Visible and High-resolution transmission electron microscopy were employed to investigate the composition and structure of the catalysts and reveal the promotion effect of gold nanoparticles on the catalytic performance and succinic acid production.

2 Experimental

2.1 Preparation of materials

All the chemicals were reagents graded and used without further purification. Succinic acid ($C_4H_6O_4$, purity > 99%, 118.09 g/mol), fumaric acid ($C_4H_4O_4$, purity > 99,116.07 g/mol), furoic acid ($C_5H_4O_3$, purity 98%,112.08 g/mol), nickel nitrate (Ni $(NO_3)_2.6H_2O$,purity > 97%, 290.79 g/mol), aluminum nitrate (Al $(NO_3)_3.9H_2O$,purity > 98,375.13 g/mol), sodium hydroxide (NaOH, purity > 97%, 40 g/mol),sodium carbonate (Na_2CO_3, purity > 99%, 105.99 g/mol) and Hydrogen peroxide (H_2O_2, 30%, 34.01 g/mol) were all purchased from sigma Aldrich. Furfural ($C_5H_4O_2$, purity 99%, 96.08 g/mol) was also purchased from Sigma Aldrich and used after distillation under reduced pressure. De-ionized water was used as a solvent throughout this study.

2.2 Preparation of Ni_xAl-LDH (x = 2,3,4)

The syntheses of carbonate-containing Ni_xAl-LDH were conducted using a constant-pH coprecipitation method [22]. The synthesis procedure was as follows: a suitable molar ratio of a metal precursor (100 mL) solution was prepared containing Ni $(NO_3)_2 6H_2O$ and Al $(NO_3)_3.9H_2O$,

and was slowly added drop wise at a rate of 0.23 mL·min^{-1} to an aqueous solution containing 0.5 M Na_2CO_3. The pH was raised to a value of 10 by the addition of 2 M NaOH. The mixture was magnetically stirred at room temperature to ensure the reaction medium homogeneity. The precipitate was isolated by centrifugation and the solid obtained was washed with distilled water many times until the excess of nitrates and carbonates was completely removed. The samples were, then, dried in an oven at 80 °C for 24 h and finally crushed to a fine powder. The samples obtained were noted as follows: Ni_xAl-LDH (x = 2,3,4).

2.3 Preparation of 1%Au/Ni_xAl-LDH (x = 2,3,4)

A deposition–precipitation method was employed to prepare the gold nanoparticles supported on Ni_xAl-LDH [44, 45].All the preparations were performed in the absence of light, known to decompose the gold precursors. An amount of 1 g of LDH support was dispersed and stirred in 20 mL of water. An aqueous solution of $AuHCl_4$ (1 mmol) was kept at pH 12 adjusted with 2.5 M NaOH solution. The gold was loaded drop wise on the synthesized hydrotalcite and then stirred for 24 h at room temperature. After filtration, the resulting solid was washed with de-ionized water. After each washing, a test with $AgNO_3$ was carried out to verify the presence of chlorides. Generally, no trace of chloride was found, after the first wash.

Finally, the resulting solid was dried at 80 °C overnight, and finally crushed to a fine powder. The LDH supported gold sample was named as 1%Au/Ni_xAl-LDH (x = 2,3,4).

2.4 General procedure for oxidation

An amount of 10 mg of the catalyst was added to the furfural solution at the concentration of 2 mmol was loaded in a three-neck round bottom flask attached with a reflux condenser and followed by the addition of 30% of hydrogen peroxide (8 mmol) as oxidant and water solvent (6 mL). The reaction was performed by stirring under atmospheric pressure at 80 °C. After the reaction, the resultant reaction mixture was diluted 20 times with water and filtered off using Millex®-LG 0.20 µm.

The reaction products were analyzed by high performance liquid chromatography (YL9100 HPLC) with UV–VIS detector using a C18 column. Sulfuric acid solution was used (H_2SO_4 10 mmol) as a mobile phase at a temperature of 30 °C.

An etaloning curve was realized for the calculation of conversion and selectivity. The conversions of all substrates were calculated by using the following formula [46] (Eq. 1):

$$\text{Conversion } (\%) = \frac{\text{substrate}_{\text{input}} - \text{substrate}_{\text{remained}}}{\text{substrate}_{\text{input}}} * 100 \quad (1)$$

Whereas the product yield selectivity was calculated by (Eq. 2)

$$\text{Selectivity } (\%) = \frac{\text{product}_{\text{detected}}}{\text{substrate}_{\text{input}}} * 100 \quad (2)$$

2.5 Characterization

The X-ray diffraction (XRD) patterns powder of the prepared samples was performed on a Rigaku diffractometer, with a copper anticathode and monochromatic graphite blade, using Cu Kα radiation (λ = 0.154 nm). The diffraction data were collected for 2 s at each 0.02 s step at 2thetas ranging from 2° to 80°. The d-spacing (d_{001}) values were calculated using Bragg's Law formula (Eq. 3).

$$n\lambda = 2d_{001}\sin\theta \quad (3)$$

The average crystallite size was calculated from the Debye–Scherrer's formula (Eq. 4).

$$D = k\lambda/\beta\cos\theta \quad (4)$$

where k is the Scherrer constant 0.9, λ the length wave of incident radiation used (nm), β the width at mid-height of the diffraction peak used (rad), and θ the Bragg diffraction angle (rad).

Fourier transform infrared spectroscopy (FTIR) spectra of samples were collected on a Perkin-Elmer 16 PC Fourier transform spectrometer equipped with a diffuse reflectance sphere. The materials were dispersed and gently ground in KBr powder, placed in the diffuse reflectance sphere, and analyzed. The results were shown in transmittance, at the range of 4000–400 cm $^{-1}$ with a resolution of 2 cm^{-1}.The texture of the synthesized materials was identified by the physical nitrogen adsorption–desorption at its liquefaction temperature (− 196 °C) on the surface of the solid degassed overnight under vacuum at 200 °C beforehand to eliminate all traces of water and CO_2.The volumetric analysis was performed using a Quantachrome Nova 1000e instrument. The measurements of the specific surface area were determined by the BET (Brunauer, Emett and Teller) method, and those of the pore distribution were determined by the BJH method. As a method for the characterization of the LDH particles, FEI NOVA SEM 450 emission scanning electron microscope operating at the optimum accelerating voltage of 2.00 kV with a resolution of 500 nm was used. The Diffuse Reflectance UV–Vis spectroscopy measurements were carried out at room temperature with JASCO UV/VIS Spectrometer in the range of 200–800 nm, the setup was equipped

with a diffuse reflectance accessory set to collect the diffuse reflected light only. High resolution transmission electron microscopy (TEM) was carried out using a field emission microscope (JEOL 2010F) operated at 300 kV. The samples were prepared by placing a drop of 5 µL of sample solution on 200 meshes of copper grids with a lacey carbon film followed by the solvent (ethanol) evaporation before transferring them into the microscope.

3 Results and discussion

3.1 Structural and textural characterization

The diffraction patterns of the prepared Ni_xAl-LDH samples in Fig. 1 section a exhibited sharp peaks at 10.7°, 22.0°, 34.1°, 38.5°, 46.4°, 60.5°, 61.5° corresponding respectively to the (003), (006), (012), (015), (018), (110) and (113) plane which are characteristic diffraction peaks of the Ni_xAl-LDH nanosheets [47–50]. The diffraction is indexed in a hexagonal system with an R3-m space group [51–53] and a rhombohedral crystal symmetry of takovite-type structure [53].

In a more in-depth exploration, the unit cell parameters and the crystallite size of the samples were evaluated and summarized in Table1.The basal spacing $d_{(003)}$ reflection values are in agreement with the presence of the carbonate anion in the interlayer region[26]. The unit cell parameter a is the average distance between two metal ions, calculated from the d-spacing of the (110) reflection with the following formula $a = 2d_{(110)}$ [21]. These values are unchanged as Al^{3+}substitutes the Ni^{2+} cations. Also, a slit change in the

Table 1 XRD parameters of the prepared materials

Catalyst	$d_{(003)}$ (Å)[a]	c (Å) [a]	a (Å) [a]	D (Å) [b]	Au (wt%) [c]
Ni_2Al-LDH	8.5	25.5	3.1	**84.22**	–
Ni_3Al-LDH	8.6	25.6	3.1	**84.21**	–
Ni_4Al-LDH	8.4	25.4	3.1	**101.07**	–
1%Au/ Ni_2Al-LDH	7.6	22.8	3.0	**71.50**	1.0
1%Au/ Ni_3Al-LDH	7.6	22.8	3.0	**83.40**	0.9
1%Au/ Ni_4Al-LDH	7.5	22.4	3.0	**83.42**	1.0

[a]Unit cell parameters calculated from XRD: $c = 3d_{(003)}$, $a = 2d_{(110)}$
[b]Crystallite size calculated from equation Debye–Scherrer $d_{(110)}$
[c]calculated from adsorption atomic spectra

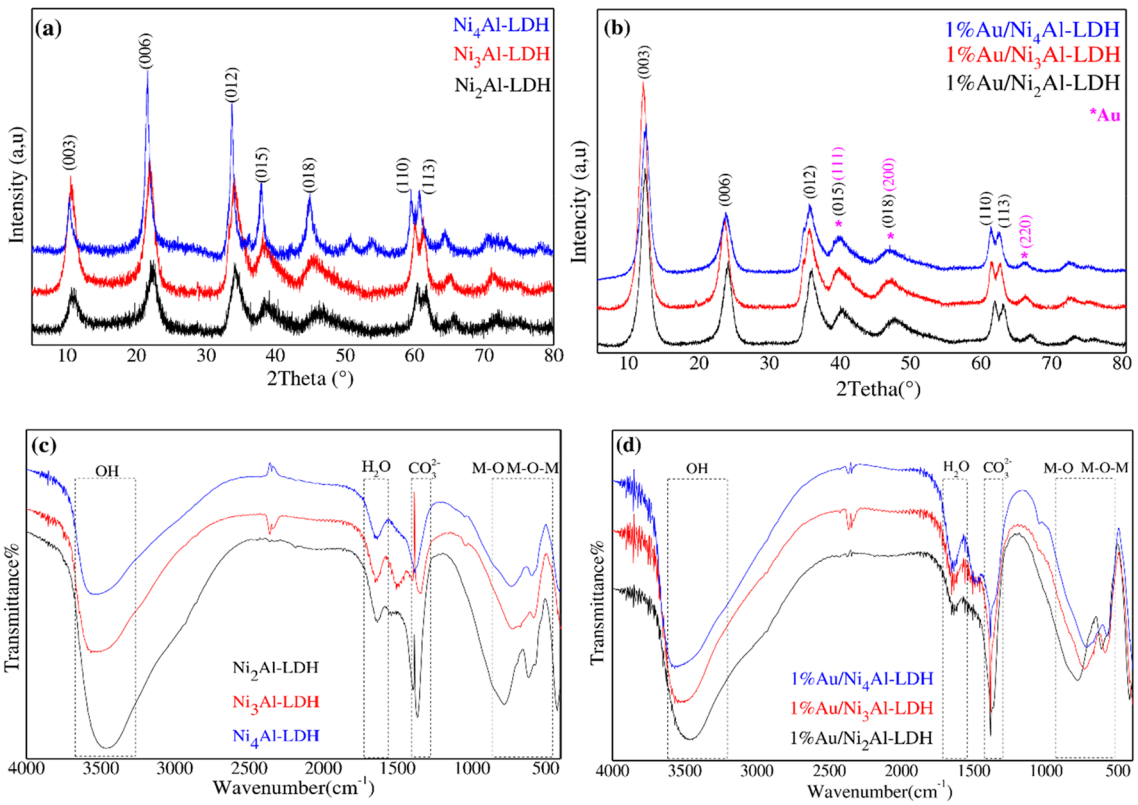

Fig. 1 XRD Analysis (**a**, **b**), FTIR spectra (**c**, **d**) of the prepared materials

crystallographic parameter *c* is visible as the Ni/Al molar ratio increase. This variation is due to the network expansion as reported by different researchers [53, 54].

The diffraction pattern peaks, as shown in Fig. 1 section b, did not change after the addition of gold nanoparticles; however the diffraction intensities were enhanced indicating that the gold supported material possesses a better general crystalline organization [31]. Nevertheless, the *c* parameter decrease suggests that gold nanoparticles may lodge on the LDH surface and not in the inter-sheet space. Moreover, the gold reflection at (111), (200) and (220) was not noticed owing to its small particle size and lower metal loading.

The Fourier transform infrared spectroscopy (FTIR) spectrum of the pristine Ni_xAl-LDH depicted in Fig. 1 section c is in agreement with the layered double hydroxide materials prepared without impurities. The following spectrum consists of a broad band located at 3300–3550 cm^{-1} confirming the presence of interlaced water molecules and OH^- group of the brucite sheet [55]. The water deformation band between 1590 and 1660 cm^{-1} confirms the presence of interstitial water molecules δ (H_2O) [21, 56, 57]. Also, an asymmetric band at 1370–1360 cm^{-1} is due to the presence of the carbonate ions interlayered within the lamellar [21, 24, 55]. As summarized in Fig. 1 section d,when the gold nanoparticles were supported over the surface of the LDH materials, no changes were observed in the FTIR spectrum [58] as it was seen on XRD diffractions. For low frequencies, the vibration bands observed are attributed to the network [59, 60], and the lattice vibration bands at 460, 590,735 cm^{-1} can be ascribed to Ni–O, Ni–O–Ni or/and Al–O–Al,Ni–OH or/and Al–OH deformation [31, 55]. These bands become sharper and clearer after the immobilization of gold nanoparticles confirming the increase of the crystallinity as observed on the XRD pattern.

The nitrogen adsorption–desorption isotherms, as well as the pore size distribution (PSD) of the hydroxide materials phases before and after the addition of gold nanoparticles were also measured and shown in Fig.S1 and Fig.S2, respectively. All the materials are of type IV, confirming their mesoporous structure with pore sizes ranging from 2 to 50 nm [61]. The isotherms show an H3 hysteresis loop type pointing out the formation of aggregates generating slit-like pores which size and shape are not uniform. The main textural parameters are compiled in Table 2 [62], from these data, it can be deduced that the specific area decreases with the Ni/Al molar ratio, from 86 to 53m^2/g, the pore volume follows a clear trend, and decreases with the Ni/Al molar ratio. The PSD profiles illustrates that both of Ni_xAl-LDH and 1%Au/Ni_xAl-LDH sample exhibit a unimodal type of distribution with a high sharp in the range of 1–25 nm with maxima of 18 nm for the initial LDH and 19 nm for the 1%Au/LDH materials, except the Ni_4Al-LDH which show a broader PSD curve with a series of non-uniform mesopores from 2 to 30 nm.

The VIS–UV spectra of the dried gold supported LDH materials were studied and shown in Fig.S12. The LDH support shows three absorption bands located at 200–300 nm, 300–500 nm and 600–800 nm. As Al^{3+} have d^0 configuration, the bans are attributed to d-d transitions of Ni^{2+} in the octahedral geometry [63, 64]. The region 200–300 nm is owing to ligand-to-metal charge transmit (O 2p → Ni 3d t_{2g}) [65]. The study of the dried 1%Au/Ni_xAl-LDH reveals the presence of bands at 213–231 nm and 328 nm characteristic of Au^{3+}, Au^+ and $Au^{\delta+}$, respectively [66]. However, the reduced Au^0 is not visible in the range 400–800 nm.

The SEM images, as illustrated in Fig.S3, indicate that the prepared lamellar hydroxide has a similar sand rose morphology with a hexagonal shape and a lateral size about 10–15 nm. This result confirms our deductions from the XRD characterization. Also, the EDS images confirm that the Ni and Al elements accounted for a large part of the Ni_xAl-LDH composition.

Figure 2 section b and Fig.S5 section b shows the transmission electron microscopy (TEM) images of the hydrotalcite supports Ni_2Al-LDH and Ni_4Al-LDH**,** respectively. The images illustrate clearly that the samples exhibit a lamellar

Table 2 Textural parameters of the prepared materials

Catalyst	BET (m^2/g)[a]	Total pore volume (cc/g)[b]	Average pore diameter[b] (nm)	Pore diameter[c] (nm)
Ni_2Al-LDH	86	0.18	18.98	8.37
Ni_3Al-LDH	83	0.14	19.13	6.74
Ni_4Al-LDH	53	0.13	18.99	9.81
1%Au/Ni_2Al-LDH	82	0.21	18.81	10.24
1%Au/Ni_3Al-LDH	92	0.17	19.03	7.39
1%Au/Ni_4Al-LDH	57	0.14	18.87	9.82

[a]Obtained by BET surface area analysis

[b]calculated from BJH pore size analysis

[c]Calculated from Gurvitsch equation Pd = $4*10^3$*(Pore volume/S_{BET})[62]

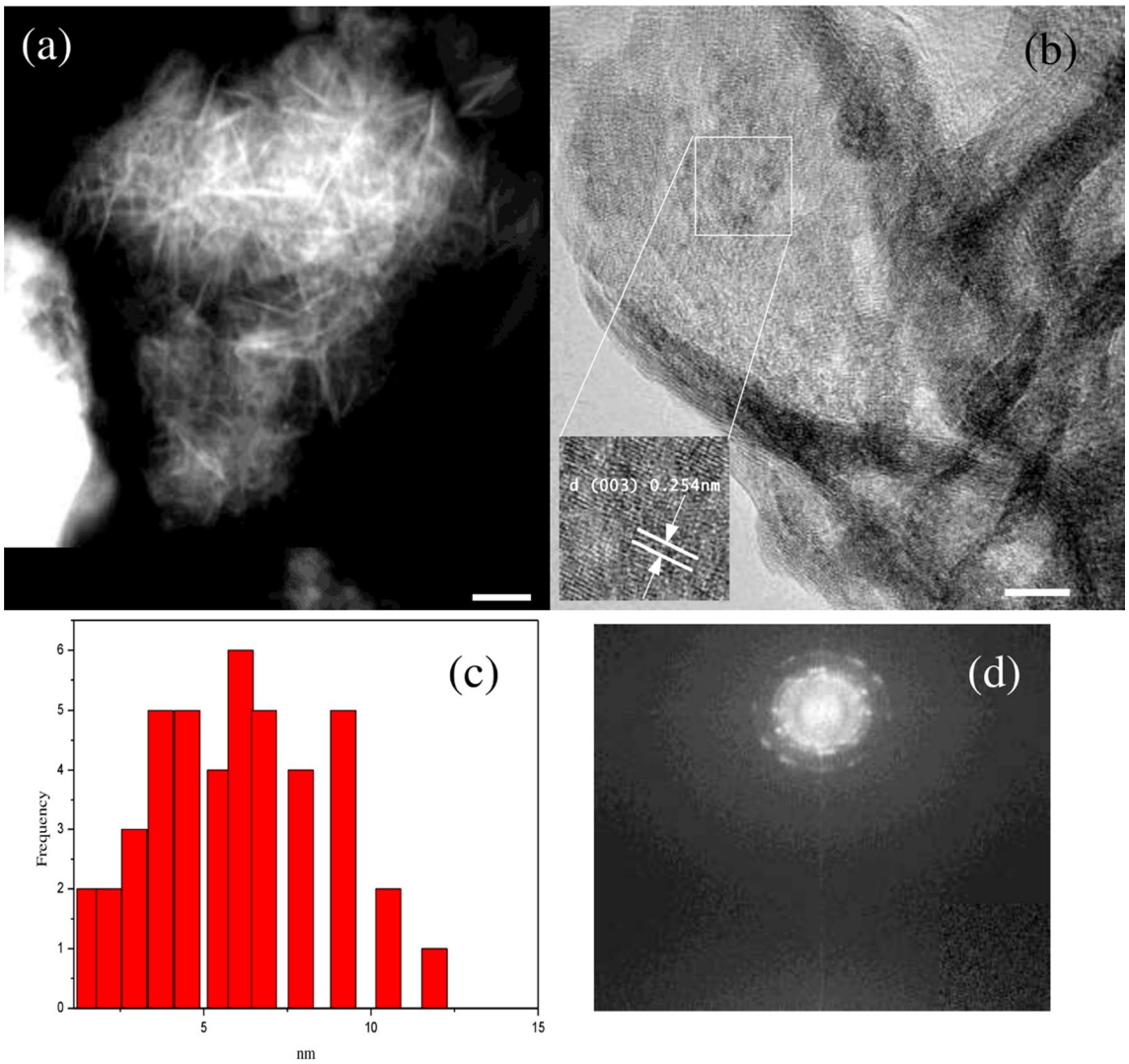

Fig.2 TEM images of **a** 1%Au/Ni_2Al-LDH, **b** Ni_2Al-LDH, **c** size histogram distribution, **d** SAED patterns of Ni_2Al-LDH

overlapping crystal structure. The plates are smooth with very thin films, crumpled and tangled, with a turbostratic disorder without any defined form in the stack layers. The lattice fringes parameters noted in white can be indexed as the (003) plane of LDH material and confirm those found by XRD calculation.

The electron diffraction diagram in Fig. 2 section d and Fig.S5 section d gives diffused and accurate spots which correspond to the reflections (hk0), and reflect the non-textured polycrystalline and turbostratic character. These diffraction rings can be ascribed to the LDH hydroxide structure [67, 68].

The supporting gold nanoparticles influence on the LDH morphological and textural properties was also investigated. The ADF-STEM images shown in Fig.S4 display that the 1%Au/Ni_xAl-LDH composites conserve the lamellar structure; however, the gold nanoparticles are hardly visible because of their low grade and small size.

Besides,the TEM microscopy, in Fig. 2 section a and Fig. S5 section a, evidenced a heterogeneous distribution of gold nanoparticles over the LDH support with a spherical shape [37] that appears as white dots on LDH surfaces highlighted that the introduction of gold does not alter the supported materials morphology.

The gold broad size distribution of the 1%Au/Ni_2Al-LDH is reported in Fig. 2 section c in more details. Most of the particles have a heterogeneous size distribution with an average diameter between 3 and 8 nm, and few of them have size in the 8–10 nm. The average diameter of gold nanoparticles was calculated to be d = 5.83 nm.

On the contrary, the 1%Au/Ni_4Al-LDH as shown in Fig. S5 section c, contains highly dispersed gold nanoparticles,

with a Gaussian shape and well evidences that most of the gold size is below 5 nm.

As a conclusion, we can say that, the results of XRD, FTIR, N_2 adsorption–desorption, SEM, UV–VIS spectra and TEM taken together evidenced the successful synthesis of 1%Au/Ni_xAl-LDH composites.

3.2 Furfural oxidation

The efficiencies of various catalysts for furfural oxidation to succinic acid in the presence of hydrogen peroxide under mild reaction parameters are shown in Fig. 3 and listed in Table 3. The reaction can give three products as shown in Fig.S6: succinic, fumaric and furoic acids [1, 13] as detected by HPLC. Regardless the catalysis composition, all the reactions achieved a maximum conversion greater than 90% after 5 h of reaction. Nevertheless, a slight difference in conversion is observed, which might be due to the changes in the morphological characteristics such as the distribution of active cites and the decrease in the specific area when the molar ratio Ni/Al increases.

The kinetic reaction progression of the LDH materials illustrated in Fig.S7, Fig.S8, Fig.S9 section a, showed an increase in furfural conversion and succinic acid selectivity with an increasing reaction time and became constant after 3 h. Fumaric acid was formed in higher amounts than succinic acid at the beginning of the reaction time and then slightly decreased. This tendency proposed that fumaric acid can be an intermediary reaction product. Also, furoic acid is formed in a law amount [1, 69]and confirms that the furfural oxidation reaction may occur without the furan ring rupture [70, 71].

On the other hand, the use of gold supported LDH has a beneficial effect on the selectivity, as shown in Fig.S7, Fig. S8, Fig.S9 section b, an unexpected behavior is observed. We notice that the use of 1%Au/Ni_2Al-LDH catalyst gives an exclusive selectivity in succinic acid production of 98%,

Table 3 Catalyst scanning for the furfural oxidation

Catalyst	Conversion%	Selectivity SA%	FA%	FuA%
Ni_2Al-LDH	92	71	16	12
Ni_3Al-LDH	96	72	17	10
Ni_4Al-LDH	91	75	16	8
1%Au/Ni_2Al-LDH	92	98	1.5	< 1
1%Au/Ni_3Al-LDH	93	53	13	33
1%Au/Ni_4Al-LDH	91	53	45	2.5
Blank	47	–	–	–

Reaction conditions: H_2O 6 mL, furfural 2 mmol, H_2O_2 8 mmol, catalyst 10 mg, 1 atm,80 °C, 24 h

while for 1%Au/Ni_3Al-LDH and 1%Au/Ni_4Al-LDH 53% of succinic acid is produced with a mixture of fumaric and furoic acid.

This unusual behavior can be attributed to the dispersion of the gold nanoparticles on the surface of the LDH support. As it is shown on TEM analysis, it can be hypothesized that the observed discrepancy between the two catalysts 1%Au/Ni_2Al-LDH and 1%Au/Ni_4Al-LDHis due to the different gold size dispersion on the support. This result indicates that there is a limiting gold nanoparticles size dividing the selectivity catalyst: where the presence of a large gold nanoparticles (size > 5 nm) in the1%Au/Ni_2AL-LDH, as shown in Fig. 2 section c, promotes the succinic acid formation. Also, the smaller gold nanoparticles (size < 4 nm) seen on the 1%Au/Ni_4AL-LDH in Fig.S5 section c, exhibit a mixing between fumaric and succinic acid. As theoretically reported, [42, 72–74] the limiting size appears to be related to an intrinsic modification of the properties of gold nanoparticles and promotes the succinic acid production.

Based on the oxidation mechanisms described in the literature [1, 75–77], two types of reaction pathway can be proposed. Fig.S10, proposes that the furan ring is opened up to

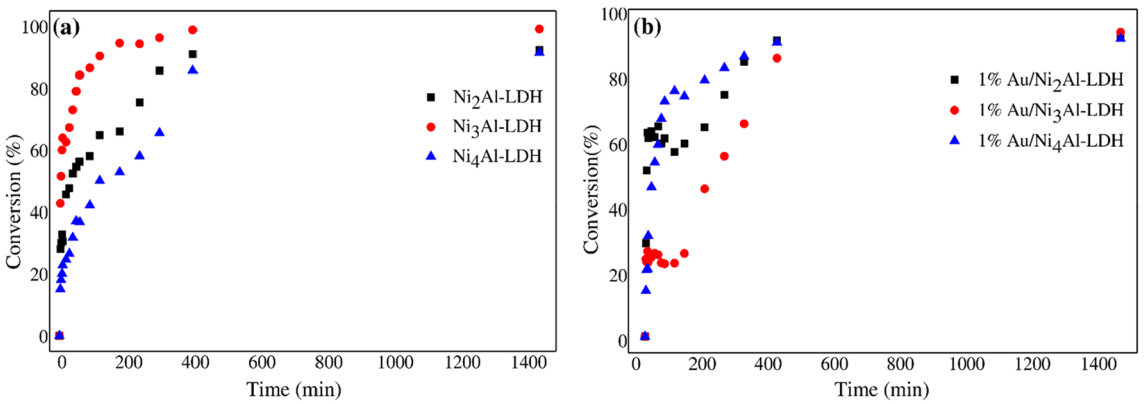

Fig.3 Reaction progress for furfural oxidation, reaction condition: H_2O 6 mL, furfural 2 mmol, H_2O_2 8 mmol, catalyst 10 mg, 1 atm, 80 °C, 24 h

forms a dienol which ketonisis to diketo aldehyde and forms succinic acid. This reaction pathway was reported by Bunton [78]on the oxidation of diketone and keto aldehyde to carboxylic acid by hydrogen peroxide, and can explain the exclusivity of succinic acid production in case of 1%Au/Ni_2Al-LDH. However, Fig.S11, involving a Bayer-Villiger oxidation step [79–81], seems more in arrangement with our results (except for 1%Au/Ni_2Al-LDH). The pathway shows that furan compound can be oxidized via furan-2(3H)-one type intermediate forming succinic acid. However, the keto-enol tautomerization of the hydrolyzed product after Bayer-Villiger oxidation can give two products: furan-2(3H)-one and furan-2(5H)-one, and can explain the fumaric acid formation [16].

4 Conclusion

In sum, we succeeded in synthesizing a series of lamellar double hydroxides and their supported gold nanoparticles, using a pH constant coprecipitation and deposition–precipitation route, respectively. An oxidation reaction was chosen to evaluate the efficiency of the catalytic activity of prepared materials. Tthese synthesized products exhibited an excellent furfural oxidation activity and a succinic acid production, especially in the presence of gold nanoparticles. These results are due to the association of gold on LDH support which promoted the succinic acid formation increase. The gold size distribution made it possible to increase the succinic acid formation exclusively when the size of this latter is up to 5 nm, whatever the smaller gold nanoparticles are to promote the formation of succinic and fumaric acids with a comparable amount.

Supplementary Information The online version contains supplementary material available at https://doi.org/10.1007/s10934-022-01325-y.

Acknowledgements The authors would like to thank the University of Tlemcen Abou Beker Belkaid, the Algerian DGRST-MESRS, and the University of Cadiz, Puerto Real for funding this work.

Author contributions GB: Investigation, Formal analysis, Validation, Conceptualization, Methodology, Writing—review & editing. RB: Conceptualization, Supervision. SB: Project administration. CJJ: Microscopy Analysis. HGJC: Microscopy analysis.

Declarations

Conflict of interest On behalf of all authors, the corresponding author states that there is no conflict of interest.

References

1. H. Choudhary, S. Nishimura, K. Ebitani, Metal-free oxidative synthesis of succinic acid from biomass-derived furan compounds using a solid acid catalyst with hydrogen peroxide. Appl. Catal. A. **458**, 55–62 (2013)
2. S.S. Dalli, T.J. Tilaye, S.K. Rakshit, Conversion of wood-based hemicellulose prehydrolysate into succinic acid using a heterogeneous acid catalyst in a biphasic system. Ind. Eng. Chem. Res. **56**(38), 10582–10590 (2017)
3. I. Bechthold et al., Succinic acid: a new platform chemical for biobased polymers from renewable resources. Chem. Eng. Technol. Ind. Chem. Plant Equip. Process Eng. Biotechnol. **31**(5), 647–654 (2008)
4. A. Zitouni et al., Production of bio-jet fuel range hydrocarbons from catalytic HDO of biobased difurfurilydene acetone over Ni/SiO2-ZrO2 catalysts. Fuel **297**, 120783 (2021)
5. W. Bendeddouche et al., Highly efficient catalytic o ne-pot biofuel production from lignocellulosic biomass derivatives. Int. J. Energy Res. **45**(2), 2148–2159 (2021)
6. T. Werpy, G. Petersen, *Top value added chemicals from biomass: volume I--results of screening for potential candidates from sugars and synthesis gas* (National Renewable Energy Lab, Golden, 2004)
7. J. Zeikus, M. Jain, P. Elankovan, Biotechnology of succinic acid production and markets for derived industrial products. Appl. Microbiol. Biotechnol. **51**(5), 545–552 (1999)
8. R. Sleat, J. Robinson, The bacteriology of anaerobic degradation of aromatic compounds. J. Appl. Bacteriol. **57**(3), 381–394 (1984)
9. C. Potera, Making succinate more successful. Natl. Inst. Environ. Health Sci. (2005). https://doi.org/10.1289/ehp.113-a832
10. M. Lomelí-Rodríguez et al., Synthesis and characterization of renewable polyester coil coatings from biomass-derived isosorbide, FDCA, 1, 5-pentanediol, succinic acid, and 1, 3-propanediol. Polymers **10**(6), 600 (2018)
11. Z. Shao et al., Aqueous-phase hydrogenation of succinic acid to γ-butyrolactone and tetrahydrofuran over Pd/C, re/C, and Pd–re/C catalysts. Ind. Eng. Chem. Res. **53**(23), 9638–9645 (2014)
12. S. Choi et al., Biorefineries for the production of top building block chemicals and their derivatives. Metab. Eng. **28**, 223–239 (2015)
13. W. Zhu et al., Efficient oxidative transformation of furfural into succinic acid over acidic metal-free graphene oxide. ACS Sustain. Chem. Eng. **7**(1), 296–305 (2018)
14. J. Akhtar, A. Idris, R.A. Aziz, Recent advances in production of succinic acid from lignocellulosic biomass. Appl. Microbiol. Biotechnol. **98**(3), 987–1000 (2014)
15. X. Li, X. Lan, T. Wang, Selective oxidation of furfural in a biphasic system with homogeneous acid catalyst. Catal. Today. **276**, 97–104 (2016)
16. H. Choudhary, S. Nishimura, K. Ebitani, Highly efficient aqueous oxidation of furfural to succinic acid using reusable heterogeneous acid catalyst with hydrogen peroxide. Chem. Lett. **41**(4), 409–411 (2012)
17. W. Kingkaew et al., Catalytic oxidation of furfural to succinic acid in the presence of sulfonic resins. Key Eng. Mater. (2020). https://doi.org/10.4028/www.scientific.net/KEM.856.182
18. M. Rezaei et al., Furfural oxidation to maleic acid with H2O2 by using vanadyl pyrophosphate and zirconium pyrophosphate supported on well-ordered mesoporous KIT-6. J. Environ. Chem. Eng. **7**(1), 102855 (2019)
19. H. Guo, G. Yin, Catalytic aerobic oxidation of renewable furfural with phosphomolybdic acid catalyst: an alternative route to maleic acid. J. Phys. Chem. C **115**(35), 17516–17522 (2011)
20. L. Zhou et al., Sulfonated carbon catalyzed oxidation of aldehydes to carboxylic acids by hydrogen peroxide. J. Energy Chem. **22**(4), 659–664 (2013)
21. K.-H. Goh, T.-T. Lim, Z. Dong, Application of layered double hydroxides for removal of oxyanions: a review. Water Res. **42**(6–7), 1343–1368 (2008)
22. S. Miyata, Physico-chemical properties of synthetic hydrotalcites in relation to composition. Clays Clay Miner. **28**(1), 50–56 (1980)

23. F. Cavani, F. Trifiro, A. Vaccari, Hydrotalcite-type anionic clays: Preparation, properties and applications. Catal. Today. **11**(2), 173–301 (1991)
24. Z. Xu, H. Zeng, Abrupt structural transformation in hydrotalcite-like compounds Mg1-x Al x (OH) 2 (NO3)x, n H2O as a continuous function of nitrate anions. J. Phys. Chem. B. **105**(9), 1743–1749 (2001)
25. V. Rives, Ma.A. Ulibarri, Layered double hydroxides (LDH) intercalated with metal coordination compounds and oxometalates. Coord. Chem. Rev. **181**(1), 61–120 (1999)
26. Š Paušová et al., Insight into the photocatalytic activity of ZnCr–CO3 LDH and derived mixed oxides. Appl. Catal. B **170**, 25–33 (2015)
27. M. Verónica et al., Ethanol steam reforming using Ni (II)-Al (III) layered double hydroxide as catalyst precursor: kinetic study. Chem. Eng. J. **138**(1–3), 602–607 (2008)
28. M. Dixit et al., Physico-chemical and catalytic properties of Mg–Al hydrotalcite and Mg–Al mixed oxide supported copper catalysts. J. Ind. Eng. Chem. **19**(2), 458–468 (2013)
29. S. Ordóñez et al., Hydrotalcite-derived mixed oxides as catalysts for different C-C bond formation reactions from bioorganic materials. Catal. Today **167**(1), 71–76 (2011)
30. C. Gomes Silva et al., Influence of excitation wavelength (UV or visible light) on the photocatalytic activity of titania containing gold nanoparticles for the generation of hydrogen or oxygen from water. J. Am. Chem. Soc. **133**(3), 595–602 (2011)
31. L. Sobhana et al., Layered double hydroxides decorated with Au-Pd nanoparticles to photodegradate orange II from water. Appl. Clay Sci. **134**, 120–127 (2016)
32. M. Haruta, Catalysis of gold nanoparticles deposited on metal oxides. CATTECH **6**(3), 102–115 (2002)
33. N. Ameur et al., Influence of nanoparticles oxidation state in gold based catalysts on the product selectivity in liquid phase oxidation of cyclohexene. J. Mol. Catal. A: Chem. **374**, 1–6 (2013)
34. Z.-Y. Cai et al., Solvent-free oxidation of cyclohexene over catalysts Au/OMS-2 and Au/La-OMS-2 with molecular oxygen. Catal. Commun. **12**(3), 197–201 (2010)
35. N. Ameur et al., Preparation and characterization of Au/Al2O3 and Au-Fe/Al2O3 materials, active and selective catalysts in oxidation of cyclohexene. Adv. Mater. Res. **856**, 48–52 (2014)
36. J. Yu et al., Hydrotalcite-supported gold catalysts for a selective aerobic oxidation of benzyl alcohol driven by visible light. J. Mol. Catal. A: Chem. **395**, 128–136 (2014)
37. L. Jin et al., Protein adsorption on gold nanoparticles supported by a layered double hydroxide. Mater. Lett **77**, 67–70 (2012)
38. L.S. SS et al., Heteronuclear nanoparticles supported hydrotalcites containing Ni (II) and Fe (III) stable photocatalysts for orange II degradation. Appl. Clay Sci. **132**, 641–649 (2016)
39. X. Liu, D. Knight, G.J. Hutchings, *Organic synthesis catalyzed by supported gold nanoparticules* (Elsevier Cardiff University, Cardiff, 2015)
40. A. Berrichi et al., Heterogeneous bimetallic Au–Co nanoparticles as new efficient catalysts for the three-component coupling reactions of amines, alkynes and CH 2 Cl 2. Res. Chem. Intermed. **45**(6), 3481–3495 (2019)
41. G. Brindley, S. Kikkawa, Thermal behavior of hydrotalcite and of anion-exchanged forms of hydrotalcite. Clays Clay Miner. **28**(2), 87–91 (1980)
42. F. Pinna et al., The effects of gold nanosize for the exploitation of furfural by selective oxidation. Catal. Today **203**, 196–201 (2013)
43. A. Corma, H. Garcia, Supported gold nanoparticles as catalysts for organic reactions. Chem. Soc. Rev. **37**(9), 2096–2126 (2008)
44. R. Zanella et al., Alternative methods for the preparation of gold nanoparticles supported on TiO2. J. Phys. Chem. B **106**(31), 7634–7642 (2002)
45. Z.-Y. Cai et al., Halloysite nanotubes supported gold catalyst for cyclohexene oxidation with molecular oxygen. Adv. Chem. Eng. Sci. **1**(1), 15–19 (2011)
46. I. Sádaba et al., Mg–Zr mixed oxides for aqueous aldol condensation of furfural with acetone: effect of preparation method and activation temperature. Catal. Today **167**(1), 77–83 (2011)
47. X. Zhang et al., A mechanochemical approach to get stunningly uniform particles of magnesium–aluminum-layered double hydroxides. Appl. Surf. Sci. **259**, 245–251 (2012)
48. J. Qu et al., Mechanochemical approaches to synthesize layered double hydroxides: a review. Appl. Clay Sci. **119**, 185–192 (2016)
49. E. Coronado et al., Intercalation of [M (ox) 3] 3−(M= Cr, Rh) complexes into NiIIFeIII-LDH. Appl. Clay Sci. **48**(1–2), 228–234 (2010)
50. M.Y. Miao, J.T. Feng, Q. Jin, Hybrid Ni-Al layred double hydroxide/ graphene composite supported gold nanoparticules for aerobic selective oxidation of benzyl alchol. Royal Soc. Chem. **5**, 36066–36074 (2015)
51. M. Gastuche, G. Brown, M. Mortland, Mixed magnesium-aluminiun hydroxides. I. Preparation and characterization of compounds formed in dialysed systems. Clay Mineral. **7**(2), 177–192 (1967)
52. G. Carja et al., The textural properties of iron substituted hydrotalcites obtained in a tailored aqueous–organic synthesis medium. Microporous Mesoporous Mater. **98**(1–3), 150–155 (2007)
53. M. Gabrovska, I. Ivanov, T. Tabakova, D. Kovacheva, 2019 Water–gas shift reaction over gold deposited on NiAl layered double hydroxides. React. Kinet. Mech. Catal. **127**, 187–203 (2019)
54. D. Guo et al., Selective aerobic oxidation of benzyl alcohol driven by visible light on gold nanoparticles supported on hydrotalcite modified by nickel ion. Catalysts **6**(5), 64 (2016)
55. R. Prikhod'ko et al., Synthesis and structural transformations of hydrotalcite-like materials Mg-Al and Zn-Al. Russ. J. Appl. Chem. **74**(10), 1621–1626 (2001)
56. P. Benito et al., Microwave-assisted reconstruction of Ni, Al hydrotalcite-like compounds. J. Solid State Chem. **181**(5), 987–996 (2008)
57. F. Millange, R.I. Walton, D. O'Hare, Time-resolved in situ X-ray diffraction study of the liquid-phase reconstruction of Mg–Al–carbonate hydrotalcite-like compounds. J. Mater. Chem. **10**(7), 1713–1720 (2000)
58. G. Rathee, S. Kohli, S. Panchal, N. Singh, A. Awasthi, S. Singh, A. Singh, S. Hooda, R. Chandra, 2020 Fabrication of a gold-supported NiAlTi-layered double hydroxide nanocatalyst for organic transformations. Am. Chem. Soc. **5**, 23967–23974 (2020)
59. M. Del Arco et al., Synthesis and characterization of hydrotalcites containing Ni (II) and Fe (III) and their calcination products. Chem. Mater. **11**(3), 624–633 (1999)
60. A.P. Kameni et al., Sensitive electrochemical detection of methyl parathion in the presence of para-nitrophenol on a glassy carbon electrode modified by a functionalized NiAl-layered double hydroxide. C. R. Chim. **22**(1), 22–33 (2019)
61. S.J. Gregg, K. Sing, *Surface area and porosity* (Academic Press Inc., Ltd, Cambridge, 1982)
62. J. Pérez-Ramírez et al., In situ investigation of the thermal decomposition of Co–Al hydrotalcite in different atmospheres. J. Mater. Chem. **11**(3), 821–830 (2001)
63. M. Holgado, V. Rives, M. SanRomán, Characterization of Ni–Mg–Al mixed oxides and their catalytic activity in oxidative dehydrogenation of n-butane and propene. Appl. Catal. A: Gen. **214**(2), 219–228 (2001)
64. Y. Wei et al., Positive Ni (HCO3) 2 as a novel cocatalyst for boosting the photocatalytic hydrogen evolution capability of mesoporous TiO2 nanocrystals. ACS Sustain. Chem. Eng. **5**(6), 5027–5038 (2017)

65. N. Baliarsingh, L. Mohapatra, K. Parida, Design and development of a visible light harvesting Ni–Zn/Cr–CO 3 2− LDH system for hydrogen evolution. J. Mater. Chem. A **1**(13), 4236–4243 (2013)
66. I. Tuzovskaya et al., Structure and electronic states of gold species in mordenites. Chem. Phys. **338**(1), 23–32 (2007)
67. Z. Liu et al., Synthesis, anion exchange, and delamination of Co− Al layered double hydroxide: assembly of the exfoliated nanosheet/polyanion composite films and magneto-optical studies. J. Am. Chem. Soc. **128**(14), 4872–4880 (2006)
68. N. Hong et al., Co-precipitation synthesis of reduced graphene oxide/NiAl-layered double hydroxide hybrid and its application in flame retarding poly (methyl methacrylate). Mater. Res. Bull. **49**, 657–664 (2014)
69. N. Alonso-Fagúndez et al., Aqueous-phase catalytic oxidation of furfural with H 2 O 2: high yield of maleic acid by using titanium silicalite-1. RSC Adv. **4**(98), 54960–54972 (2014)
70. F. Saleem et al., Kinetics and modelling of furfural oxidation with hydrogen peroxide over a fibrous heterogeneous catalyst: effect of reaction parameters on yields of succinic acid. J. Chem. Technol. Biotechnol. **92**(9), 2206–2220 (2017)
71. M.J. da Silva, A.A. Rodrigues, Metal silicotungstate salts as catalysts in furfural oxidation reactions with hydrogen peroxide. Molecular Catalysis **493**, 111104 (2020)
72. O. Casanova, S. Iborra, A. Corma, Biomass into chemicals: one pote-base free oxidative esterification of 5-hydroxymethyl-2-furfural into 2,5-dimethylfuroate with gold on nanoparticulated ceria. J. Catal. **265**(1), 109–116 (2009)
73. A. Roldán, J.M. Ricart, F. Illas, G. Pacchioni, O2 adsorption and dissociation on neutral, positively and negatively charged Au_n (n=5-79) clusters. Phys. Chem. Chem. Phys. (2010). https://doi.org/10.1039/c004110f
74. M. Turner, V.B. Golovko, O.P. Vaughan, P. Abdulkin, A. Berenguer-Murcia, M.S. Tikhov, B.F. Johnson, R.M. Lambert, selective oxidation with dioxygen by gold nanoparticle catalysts derived from 55-atom clusters. Nature **454**(7207), 981–983 (2008)
75. N.A. Milas, W.L. Walsh, Catalytic oxidations. I. Oxidations in the furan series. J. Am. Chem. Soc. **57**(8), 1389–1393 (1935)
76. G. Muzychenko, L. Badovskaya, V. Kul'nevich, Role of water in the oxidation of furfural with hydrogen peroxide. Chem. Heterocycl. Compd. **8**(11), 1311–1313 (1972)
77. V.G. Kul'nevich, L.A. Badovskaya, Reactions of oxo-derivatives of furan with hydrogen peroxide and peroxy-acids. Russ Chem. Rev. **44**(7), 574 (1975)
78. C. Bunton, Oxidation of α-diketones andα-keto-acids by hydrogen peroxide. Nature **163**(4142), 444–444 (1949)
79. A. Baeyer, V. Villiger, Einwirkung des caro'schen reagens auf ketone. Ber. Dtsch. Chem. Ges. **32**(3), 3625–3633 (1899)
80. J.W. Westley et al., Isolation and characterization of the first halogen containing polyether antibiotic, a product of streptomyces malachitofuscus subsp. Downeyi. J. Antibiot. **34**(2), 139–147 (1981)
81. C. Jiménez-Sanchidrián et al., Baeyer-Villiger oxidation of cyclohexanone with hydrogen peroxide/benzonitrile over hydrotalcites as catalysts. Appl. Catal. A **312**, 86–94 (2006)